Postprocessing of Corbino-Castillo mimetic difference solutions for error estimation*

Jhabriel Varela and Miguel A. Dumett

May 12, 2025

Publication Number: CSRCR2025-03

Computational Science & Engineering Faculty and Students Research Articles

Database Powered by the Computational Science Research Center Computing Group & Visualization Lab

COMPUTATIONAL SCIENCE & ENGINEERING

SAN DIEGO STATE UNIVERSITY

Computational Science Research Center
College of Sciences
5500 Campanile Drive
San Diego, CA 92182-1245
(619) 594-3430

Postprocessing of Corbino-Castillo mimetic difference solutions for error estimation*

Jhabriel Varela[†‡] Miguel A. Dumett[§]

May 12, 2025

1 Introduction

A posteriori error analysis unlocks the possibility of estimating errors associated to the approximate solution to a Partial Differential Equation (PDE) or a system of PDEs. One can then use these error indicators to selectively refine regions of large errors and/or coarsen regions of small errors. This process usually takes place within an Adaptive Mesh Refinement/Coarsening (AMR/C) routine. Naturally, this is considerably attractive, as one can obtain significant computational savings.

One such a class of *a posteriori* error analysis is the energy-based *a posteriori* error analysis, where one measures the difference between an approximation to the exact solution and the exact solution in the same *energy* space [1, 2, 3]. The energy space for the primal variable (commonly the pressure, temperature, concentration, etc) is a subspace of the $H^1(\Omega)$ space, whereas the energy space for the dual variable (commonly a flux associated to the gradient of the primary variable via some constitutive law) is a subspace of the $\mathbf{H}(\text{div}, \Omega)$ space.

In this report, we show how to perform lowest-order postprocessing of the mimetic difference solutions and obtain energy-conforming potentials and fluxes, which are suitable for energy-based *a posteriori* error analysis.

*JV was funded by CONACYT through Project PRIA01-8: *Insertion of Advanced Human Capital in Academia*. This work was also partially supported by SDSU.

[†]Polytechnic School, National University of Asunción (jhabriel@pol.una.py)

[‡]Polytechnic University Taiwan-Paraguay (jvarela@uptp.edu.py)

[§]Computational Science Research Center at the San Diego State University (mdumett@sdsu.edu).

The outline of this report is the following: In Section 2 we present the model problem, in Section 3 its mimetic discretization, and in Section 4 the proposed postprocessing of potentials and fluxes. Finally, in Section 5, we show a convergence analysis using a manufactured solution, and in Section 6 we draw our conclusions and discuss possible extensions.

2 The model problem

Let $\Omega \subset \mathbb{R}^2$, be an open and bounded domain whose boundary $\Gamma \subset \mathbb{R}$ is sufficiently smooth. We begin by stating the strong form of the model problem.

Definition 1 (Strong primal form)**.** *Find the potential* $p : \Omega \to \mathbb{R}$ *such that*

$$\nabla \cdot (-\nabla p) = f \quad \text{in } \Omega, \tag{1a}$$

$$p = 0 \quad \text{on } \Gamma. \tag{1b}$$

In Definition 1, ∇ is the usual *nabla* operator and $f : \Omega \to \mathbb{R}$ is a given source term. The term $-\nabla p$ represents the exact flux $\mathbf{u}$ associated to the gradient of the potential.

Instead of working with the strong form of the problem, we shall introduce its weak version. To this aim, we begin by recalling the standard Sobolev spaces. Let $H^1(\Omega) = \{q \in L^2(\Omega) : \nabla q \in [L^2(\Omega)]^2\}$ be the usual energy space, with $H^1_0(\Omega) = \{q \in H^1(\Omega) : q = 0 \text{ on } \Gamma\}$ denoting the energy space with vanishing traces on the boundary of the domain. We will also need the space of square-integrable vector functions with square integrable weak divergence: $\mathbf{H}(\mathrm{div}, \Omega) = \{\mathbf{v} \in [L^2(\Omega)]^2 : \nabla \cdot \mathbf{v} \in L^2(\Omega)\}$.

We are now ready to define the weak form of Definition 1:

Definition 2 (Primal weak form)**.** *Let* $f \in L^2(\Omega)$*. Then, find* $p \in H^1_0(\Omega)$ *such that*

$$(\nabla p, q)_\Omega = (f, q)_\Omega \quad \forall\ q \in H^1_0(\Omega). \tag{2}$$

It is well known that the primal weak form from Definition 2 admits a unique solution by the Lax-Millgram lemma. A typical energy-based upper bound on the primal variable, will have the form

$$|||p - q||| := \|\nabla(p - q)\|_\Omega \leqslant \mathfrak{M}(q, \mathbf{v}, f), \quad \forall q \in H^1_0(\Omega), \mathbf{v} \in \mathbf{H}(\mathrm{div}, \Omega), \tag{3}$$

where $|||\cdot|||$ is the energy-norm and $\mathfrak{M} : H_0^1(\Omega) \to \mathbb{R}$ is the functional defining the upper bound on the error. Thus, to be able to measure the error, we must have access to $q \in H_0^1(\Omega)$ and $\mathbf{v} \in \mathbf{H}(\mathrm{div}, \Omega)$. Although these can be arbitrary functions, in practice, we construct q and $\mathbf{v}$ from the approximated potential and flux obtained from the numerical solution.

3 Mimetic difference approximation

Let us now introduce $\mathcal{T}_h$, the decomposition of the domain Ω into strictly non-overlapping subdomains K of dimension 2. That is,

$$\overline{\Omega} = \bigcup_{K \in \mathcal{T}_h} K. \tag{4}$$

For simplicity of exposition, we assume that all elements $K \in \mathcal{T}_h$ are squares. In other words, we will be restricting our analysis to Cartesian grids as the one shown in Figure (1).

Mimetic differential operators [4, 5, 6, 7] are constructed as discrete counterparts of the continuous operators ∇, $\nabla\cdot$, ∇^2. $\nabla\times$, satisfying identities from vector calculus. In this report, we focus on a specific type of mimetic discretization, i.e., the one obtained using mimetic operators of the Corbino-Castillo type [8]. Mimetic difference operators of the Corbino-Castillo type, on top of preserving identities from continuous vector calculus, provide higher-order difference operators that attain the same level of accuracy in the interior of the domain and on its boundaries. These operators are defined on a staggered grid (see, e.g., Figure 1), where potentials (red dots) and fluxes (blue diamonds) are approximated in different locations.

Denote by $\mathcal{P}$ the set of primal degrees of freedoms (DoFs) and by $\mathcal{F}$ the set of dual DoFs. Then, one can define the gradient operator $G : \mathbb{R}^{|\mathcal{P}|} \to \mathbb{R}^{|\mathcal{F}|}$, the divergence operator $\mathbb{R}^{|\mathcal{F}|} \to \mathbb{R}^{|\mathcal{P}|}$, the Laplacian operator $L := D \circ G : \mathbb{R}^{|\mathcal{P}|} \to \mathbb{R}^{|\mathcal{P}|}$, and the boundary operator $B = \mathbb{R}^{|\mathcal{P}|} \to \mathbb{R}^{|\mathcal{P}|}$ (enforcing Dirichlet boundary conditions). These mappings have well-defined matrix representations $[G] \in \mathbb{R}^{|\mathcal{F}|\times|\mathcal{P}|}$, $[D] \in \mathbb{R}^{|\mathcal{P}|\times|\mathcal{F}|}$, $[L] \in \mathbb{R}^{|\mathcal{P}|\times|\mathcal{P}|}$, and $[B] \in \mathbb{R}^{|\mathcal{P}|\times|\mathcal{P}|}$. The explicit forms of these matrices will depend on the order of accuracy k of the mimetic operator. Thus, we will naturally have different matrices for mimetic operators with different orders of accuracy. Below, we show an example of the gradient matrix for $k = 2$.

Example 1 (Mimetic gradient matrix for $k = 2$)**.** *Let h denote the width of a cell $K \in \mathcal{T}_h$, then the second-order accurate mimetic gradient matrix is*

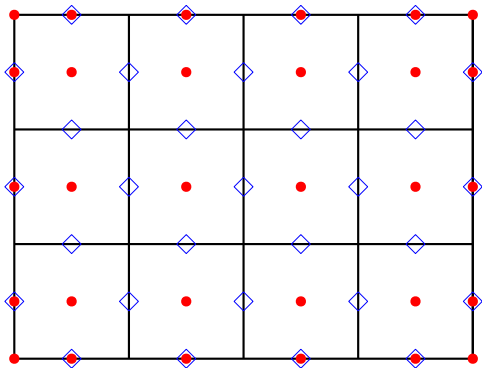

Figure 1: A 4 by 3 staggered grid. In red dots, we show the degrees of freedoms associated to the primal variable (i.e., the potential). In blue diamonds, we show the degrees of freedoms associated to the dual variable (i.e., the flux).

given by

$$[G]^{(2)} := \frac{1}{h}\begin{bmatrix} -\frac{8}{3} & 3 & -\frac{1}{3} & & & \\ & -1 & 1 & & & \\ & & \ddots & \ddots & & \\ & & & -1 & 1 & \\ & & & \frac{1}{3} & -3 & \frac{8}{3} \end{bmatrix} \tag{5}$$

Remark 1. *A full suite of mimetic difference operators for $k \in \{2,4,6,8\}$ is available in the MOLE library [9].*

With the mimetic difference matrices at hand, the mimetic approximation can be now be defined.

Definition 3 (Mimetic difference approximation to the Poisson problem)**.** *Let $k \in \{2,4,6,8\}$ be fixed and $[G]^{(k)}$, $[L]^{(k)}$, $[B]^{(k)}$ available. Then, find $\boldsymbol{p}_h := \{p_{h,1}, \ldots, p_{h,|\mathcal{P}|}\} \in \mathbb{R}^{|\mathcal{P}|}$ and $\mathbf{u}_h := \{u_{h,1}, \ldots, u_{h,|\mathcal{F}|}\} \in \mathbb{R}^{|\mathcal{F}|}$ such that*

$$\left([L]^{(k)} + [B]^{(k)}\right)\boldsymbol{p}_h = \boldsymbol{f}, \tag{6}$$

$$\boldsymbol{u}_h = -[G]^{(k)}\boldsymbol{p}_h, \tag{7}$$

where $\boldsymbol{f} = \{f_1, \ldots, f_{|\mathcal{P}|}\}$ is the exact source term projected onto the primal DoFs nodes.

Since the primal mimetic solution is only defined on the cell centers and the dual mimetic solution on the face centers, we are required to postprocess

both solutions to obtain functions that are in the correct energy spaces, namely $H_0^1(\Omega)$ and $\mathbf{H}(\mathrm{div}, \Omega)$. To this aim, we leverage on the theory of broken finite element spaces, in particular on the isoparametric elements for the potentials and Raviart-Thomas elements for the flux.

4 Postprocessing of the mimetic solution

4.1 Local broken spaces

Before introducing the postprocessing techniques, we need to introduce the relevant local finite element spaces [10]. We use $\mathbb{P}_s(K)$ to denote the space of polynomial functions of degree $\leqslant s$ on K. For a rectangular element K, we also need

$$\mathbb{P}_{s_1,s_2}(K) = \left\{ q(x,y) : q(x,y) = \sum_{\substack{i \leqslant s_1 \\ j \leqslant s_2}} a_{ij} x^i y^j \right\},$$

the space of polynomials of degree $\leqslant s_1$ in x and $\leqslant s_2$ in y. The local isoparametric space of degree s or less is then given by $\mathbb{Q}_s(K) = \mathbb{P}_{s,s}(K)$.

For postprocessing the dual variable, we will need the Raviart-Thomas spaces of degree s, which for quadrilaterals are given by

$$\mathbb{RT}_s(K) = \mathbb{P}_{s+1,s} \times \mathbb{P}_{s,s+1}, \quad s \geqslant 0, \tag{8}$$

of dimension $2(s+1)(s+2)$. Importantly, for any vector-valued function $\mathbf{v} \in \mathbb{R}^2$, there holds for all $K \in \mathcal{T}_h$:

$$\nabla \cdot \mathbf{v}|_K \in \mathbb{Q}_s(K) \quad \text{and} \quad \mathbf{v} \cdot \mathbf{n}|_e \in \mathbb{P}_s(e) \ \forall \ e \in \mathcal{E}_K, \tag{9}$$

where e is the edge of the set of edges $\mathcal{E}_K$ associated to the element K.

Example 2 (The space $\mathbb{Q}_1(K)$)**.** *Let K be a quadrilateral domain. Then, any scalar function $q \in \mathbb{Q}_1(K)$ satisfies*

$$q(x,y) = a + bx + cy + dxy, \quad a,b,c,d \in \mathbb{R}. \tag{10}$$

Example 3 (The space $\mathbb{RT}_0(K)$)**.** *Let K be a quadrilateral domain. Then, any vector function $\mathbf{v} \in \mathbb{RT}_0(K)$ satisfies*

$$\mathbf{v}(x,y) = \begin{bmatrix} a + bx \\ c + dy \end{bmatrix}, \qquad a,b,c,d \in \mathbb{R}. \tag{11}$$

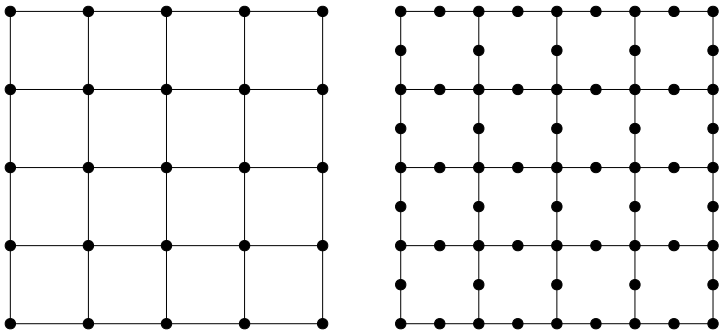

Figure 2: Degrees of freedom needed to perform a local $\mathbb{Q}_1$ (left), and a local $\mathbb{Q}_2$ reconstruction (right).

With the local finite-element spaces defined, we can now construct the global broken spaces

$$\mathbb{Q}_s(\mathcal{T}_h) = \{q \in L^2(\Omega) : q|_K \in \mathbb{Q}_s(K) \ \forall \ K \in \mathcal{T}_h\} \tag{12}$$

$$\mathbb{RT}_s(\mathcal{T}_h) = \{\mathbf{q} \in [L^2(\Omega)]^2 : \mathbf{q}|_K \in \mathbb{RT}_s(K) \ \forall \ K \in \mathcal{T}_h\} \tag{13}$$

It can be checked that $\mathbb{Q}_s(\mathcal{T}_h) \cap H_0^1(\Omega)$ is a subspace of $H_0^1(\Omega)$ for any $s \geqslant 1$. On the other hand, one can also show that $\mathbb{RT}_s(\mathcal{T}_h) \subset \mathbf{H}(\mathrm{div}, \Omega)$ for any $s \geqslant 0$.

4.2 Postprocessing

From the previous discussion, we conclude that we must define two global interpolants, one for the primal mimetic solution and one for the dual mimetic solution. To be precise, for the primal mimetic solution, we seek for an interpolant

$$\mathcal{G}_{\mathcal{P}}^{(s)} : \mathbb{R}^{|\mathcal{P}|} \to \mathbb{Q}_s(\mathcal{T}_h) \cap H_0^1(\Omega), \quad s \geqslant 1, \tag{14}$$

whereas for the dual mimetic solution, we seek for an interpolant

$$\mathcal{G}_{\mathcal{F}}^{(s)} : \mathbb{R}^{|\mathcal{F}|} \to \mathbb{RT}_s(\mathcal{T}_h), \quad s \geqslant 0. \tag{15}$$

We shall now provide specific definitions for $\mathcal{G}_{\mathcal{P}}^{(1)}$ and $\mathcal{G}_{\mathcal{F}}^{(0)}$. Higher-order interpolants can be defined analogously. However, it is important to remark three important points:

1. Since the cost of estimating the error must be a small fraction of solving a new linear system (6), one should be cautious in the use of

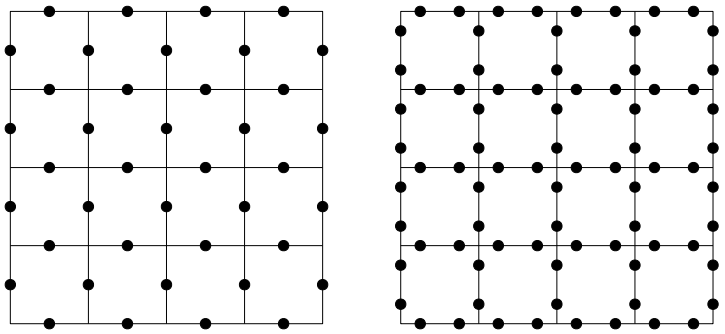

Figure 3: Degrees of freedom needed to perform a local $\mathbb{RT}_0$ reconstruction (left), and a local $\mathbb{RT}_1$ reconstruction (right).

higher-order interpolants, as they naturally require more data points (see the increase in data points in Figures 2 and 3).

2. Most upper bounds (3) assume that the postprocessing process is "error-free". Thus, one should avoid introducing interpolation errors while interpolating the mimetic solution for generating the local data points. For higher-order mimetic schemes, this demands for interpolants of the same order as k.

3. As the interpolant order s increases, one needs to interpolate the mimetic solution at non-standard locations (see e.g., the $\mathbb{RT}_1$ reconstruction from the right panel of Figure 3). This requires "generic" interpolants as proposed in [11].

Before presenting the potential reconstruction, we need a few more ingredients. Let $\mathcal{V}$ be the set of vertices of $\mathcal{T}_h$ and let $[I_{\mathcal{P}\to\mathcal{V}}]^{(k)} \in \mathbb{R}^{|\mathcal{V}|\times|\mathcal{P}|}$ be the matrix representation of the mimetic interpolant $I_{\mathcal{P}\to\mathcal{V}} : \mathbb{R}^{|\mathcal{P}|} \to \mathbb{R}^{|\mathcal{V}|}$, mapping from primal DoFs to vertices DoFs.

Definition 4 (Lowest-order potential reconstruction)**.** *Let $\boldsymbol{p}_h \in \mathbb{R}^{|\mathcal{P}|}$ be the vector of cell-center pressures, and define the nodal vector*

$$\boldsymbol{p}_V \;=\; [I^{(k)}_{\mathcal{P}\to\mathcal{V}}]\,\boldsymbol{p}_h \;\in\; \mathbb{R}^{|\mathcal{V}|}. \tag{16}$$

Then the reconstructed potential $\tilde{p}_h$ is the unique continuous piecewise–bilinear function $\tilde{p}_h \in \mathbb{Q}_1(\mathcal{T}_h) \cap H^1_0(\Omega)$ whose restriction to each quadrilateral K is

$$\tilde{p}_h\big|_K(x,y) = \sum_{i=1}^{4} (\boldsymbol{p}_V)_i\, \phi_{V_i}(x,y), \tag{17}$$

where $\{\phi_{V_i}\}_{i=1}^4$ *are the local bilinear (hat) basis functions for the vertices of* K*.*

We now consider the case of the dual mimetic variable, i.e., the flux. In the lowest-order case, we already have the necessary data points to perform the reconstruction. Thus, we simply need to extend the edge fluxes into the interior of each cell with the help of Raviart-Thomas basis functions.

Definition 5 (Lowest-order flux reconstruction)**.** *Let* $\boldsymbol{u}_h \in \mathbb{R}^{|F|}$ *be the vector of edge-centered fluxes. Then the reconstructed flux* $\tilde{\mathbf{u}}_h$ *is the unique vector function* $\tilde{\mathbf{u}}_h \in \mathbb{RT}_0(\mathcal{T}_h)$ *whose restriction to each quadrilateral* K *is*

$$\tilde{\mathbf{u}}_h|_K(x,y) = \sum_{i=1}^{4} (\tilde{\mathbf{u}}_h)_j \boldsymbol{\psi}_j(x,y), \tag{18}$$

where $\{\boldsymbol{\psi}_j\}_{j=1}^4$ *are the local Raviart-Thomas basis functions for the edges of* K*.*

5 Numerical results

Let us now test against a manufactured solution the proposed reconstruction techniques. To this aim, we consider a smooth trigonometric solution, given by

$$p(x,y) = \sin(\pi x)\cos(\pi y).$$

Taking the negative gradient of $p(x,y)$, we obtain the exact flux given by

$$\mathbf{u}(x,y) = \begin{bmatrix} \pi\cos(\pi x)\sin(\pi y) \\ \pi\cos(\pi x)\sin(\pi y) \end{bmatrix}.$$

The divergence of $\mathbf{u}(x,y)$, corresponds to the exact source term

$$f(x,y) = 2\pi^2 \sin(\pi x)\cos(\pi y).$$

This source term $f(x,y)$ can be used in the computational code to obtain the mimetic solutions $\boldsymbol{p}_h$ and $\boldsymbol{u}_h$. Having these available, we employ Definition 4 to reconstruct the potential and Definition 5 to reconstruct the flux. In Figure 4, we show the exact and reconstructed potential solutions and in Figure 5, we show the exact and reconstructed magnitude of the flux solutions. The plots, obtained with a 40x40 grid and mimetic operators of order 2, are qualitatively identical.

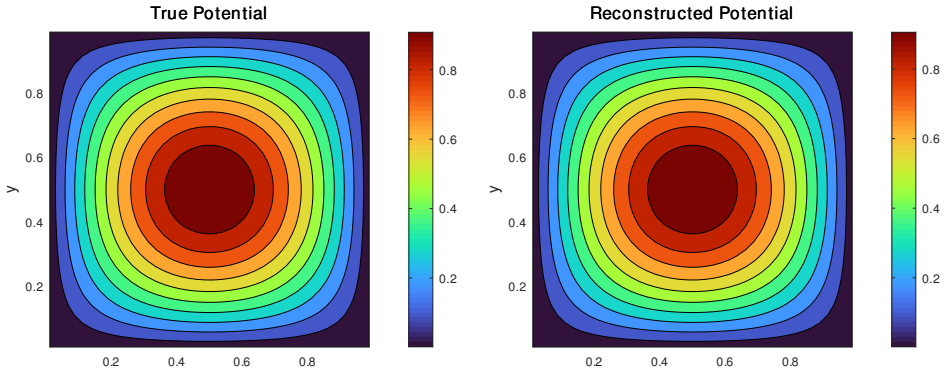

Figure 4: True vs reconstructed potentials for a 40x40 Cartesian grid with mimetic operators of order $k = 2$.

To perform a quantitative analysis, we measure the errors for the potential and the flux in the following norms:

$$\text{Error potential} := |||p - \tilde{p}_h|||, \quad \text{Error flux} := \|\mathbf{u} - \tilde{\mathbf{u}}_h\|.$$

The errors are measured for successively refined values of h, namely $h \in \{\frac{0.1}{2^i}\}_{i=0}^{5}$. The convergence analysis is shown in Figure 6. We can see that for both, the primal and dual variables, the errors decrease linearly, as expected for energy norms.

6 Conclusion and Outlook

In this technical report, we have proposed concrete procedures to reconstruct the potentials and fluxes obtained from the numerical solution to the Poisson equation with Corbino-Castillo mimetic operators.

Numerical examples for two-dimensional Cartesian grids using a smooth manufactured solution show optimal convergence rates of $\mathcal{O}(h)$ for the gradient of the reconstructed potential and the reconstructed flux, in the case of lowest-order reconstructions using mimetic operators of order $k = 2$.

Natural extensions of this work include using the postprocessing techniques in a *a posteriori* analysis and adaptive mesh refinement. Paths worth exploring include: (i) more complex PDEs, (ii) trade-off between using higher-order interpolants and computational cost, and (iii) $h-k$ adaptivity.

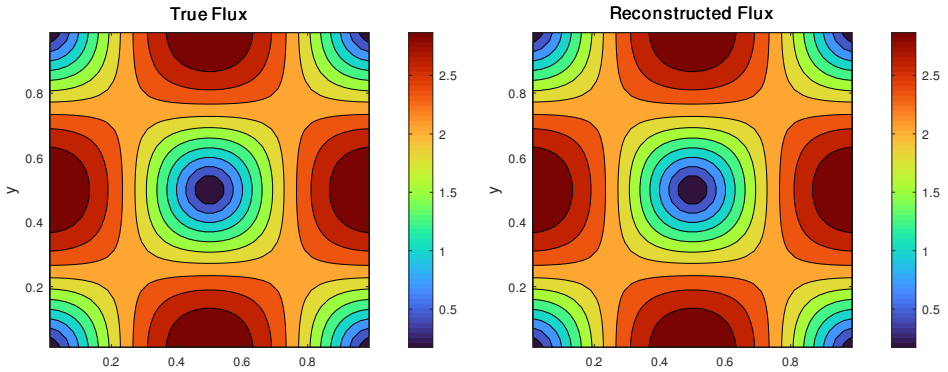

Figure 5: True vs reconstructed fluxes for a 40x40 Cartesian grid with mimetic operators of order $k = 2$.

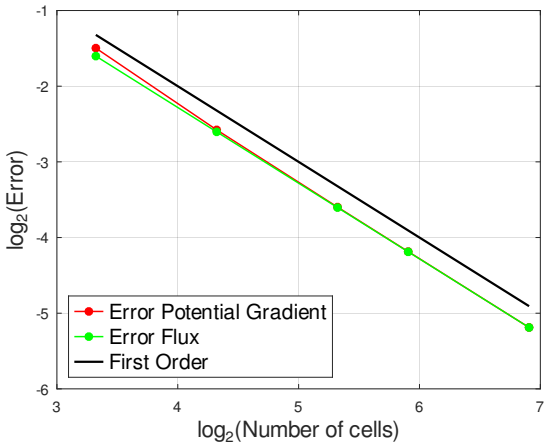

Figure 6: Convergence analysis for five levels of refinement. Optimal (first order) convergence rates are obtained for the gradient of the reconstructed potential and the reconstructed flux.

References

[1] Sergey Repin. *A posteriori estimates for partial differential equations*. Walter de Gruyter, 2008.

[2] Martin Vohralík. Unified primal formulation-based a priori and a posteriori error analysis of mixed finite element methods. *Mathematics of computation*, 79(272):2001–2032, 2010.

[3] Alexandre Ern and Martin Vohralík. Polynomial-degree-robust a posteriori estimates in a unified setting for conforming, nonconforming, discontinuous galerkin, and mixed discretizations. *SIAM Journal on Numerical Analysis*, 53(2):1058–1081, 2015.

[4] Konstantin Lipnikov, Gianmarco Manzini, and Mikhail Shashkov. Mimetic finite difference method. *Journal of Computational Physics*, 257:1163–1227, 2014.

[5] Lourenço Beirao da Veiga, Konstantin Lipnikov, and Gianmarco Manzini. *The mimetic finite difference method for elliptic problems*, volume 11. Springer, 2014.

[6] José E Castillo and Guillermo F Miranda. *Mimetic discretization methods*. CRC Press, 2013.

[7] Anand Srinivasan, Miguel Dumett, Christopher Paolini, Guillermo F Miranda, and José E Castillo. Mimetic finite difference operators and higher order quadratures. *GEM-International Journal on Geomathematics*, 14(1):19, 2023.

[8] Johnny Corbino and Jose E Castillo. High-order mimetic finite-difference operators satisfying the extended gauss divergence theorem. *Journal of Computational and Applied Mathematics*, 364:112326, 2020.

[9] Johnny Corbino, Miguel A Dumett, and Jose E Castillo. Mole: Mimetic operators library enhanced. *Journal of Open Source Software*, 9(99):6288, 2024.

[10] Daniele Boffi, Franco Brezzi, Michel Fortin, et al. *Mixed finite element methods and applications*, volume 44. Springer, 2013.

[11] M. A. Dumett. High-order interpolants for derivatives of smooth functions restricted to hexahedral nodes. Technical Report CSRCR2024-09, Computational Science Research Center, San Diego State University, December 2024.